DOI: 10.1002/ejic.200500792

Synthesis, Characterization, and Properties of Some Copper(II) Complexes of 2-Pyridineformamide Thiosemicarbazone (HAm4DH)

María del Carmen Aguirre,[a] Joaquín Borrás,[b] Alfonso Castiñeiras,*[a] José M. García-Monteagudo[c] Isabel García-Santos,[a] Juan Niclós,[d] and Douglas X. West[e]

Keywords: Thiosemicarbazones / Copper complexes / One-dimensional chains / Cyclic voltammetry / DNA cleavage

Reactions between different copper(II) salts and 2-pyridineformamide thiosemicarbazone (HAm4DH) in neutral ethanolic media led to the formation of complexes with the formulae $[Cu(HAm4DH)X_2]$ (X = Cl or Br) (**1**, **2**) and $[Cu(HAm4DH)_2]X_2$ (X = NO_3 or ClO_4) (**3**, **4**). The same reactions carried out in the presence of triethylamine gave rise to new complexes with the general formulae [Cu(Am4DH)X] (X = Cl, Br, AcO, or NO_3) (**5**–**8**), $[Cu(H_2O)(Am4DH)](ClO_4)$ (**9**), and $[Cu(Am4DH)_2]$ (**10**), many of which were isolated with different molecules of crystallization and contain a deprotonated thiosemicarbazone (Am4DH). These complexes were characterized by elemental analysis, and different spectroscopic and magnetic techniques. The thermal and redox behavior of the complexes was also evaluated. Complexes **1**, **2**, **5**, and **6** show better nuclease activity than $[Cu(phen)_2]^{2+}$. In addition, crystals were isolated in the cases of $[Cu(HAm4DH)Cl_2]_2$ (**5a**), $^1_\infty$[Cu(Am4DH)Cl] (**5b**), $^1_\infty$[Cu(Am4DH)Br] (**6a**), and $[Cu(HAm4DH)(H_2O)(ClO_4)_2]\cdot MeOH\cdot H_2O$ (**9a**) and these structures were analyzed by X-ray diffraction. Compound **5a** has a dimeric structure with chlorine bridges and shows weak antiferromagnetism (J = –12.2 cm^{-1}). Complexes **5b** and **6a** are one-dimensional polymers formed through halogen bridges and the deprotonated thiosemicarbazone in the thiolate form. In compound **9a** the copper(II) is in a distorted octahedral environment with two ClO_4 units coordinated to the metal center.

Introduction

In general, thiosemicarbazones are obtained by condensation of the corresponding thiosemicarbazide with aldehydes or ketones.[1] However, an alternative method of synthesis involves the use of nitriles as starting materials.[2] In this case, the resulting thiosemicarbazones contain an additional amino group (Scheme 1), which gives improved water solubility. This in turn can improve the biological activity of these compounds and their metal complexes. Furthermore, this amino group is undoubtedly able to participate in hydrogen bond formation, which can favor the formation of supramolecular species.

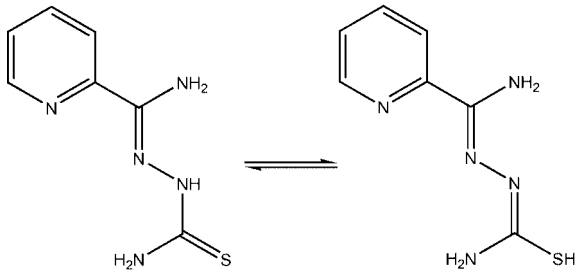

Ia **Ib**

Scheme 1.

Thiosemicarbazones in the solid state are in an approximately planar arrangement with a *Z* configuration around the C=N bond and the terminal thioamide sulfur atom in a *trans* disposition with respect to the azomethine nitrogen (**Ia** in Scheme 1). The fact that this system undergoes *thione–thiol* tautomerism makes the thiosemicarbazones versatile ligands for a wide range of metal ions both in the neutral and anionic forms (Scheme 1).

Thiosemicarbazones generally coordinate to metal centers through the sulfur and azomethine nitrogen atoms to give a five-membered chelate ring with the metal. The resulting complexes are usually mononuclear,[3] dinuclear,[4,5]

[a] Departamento de Química Inorgánica, Facultad de Farmacia, Universidad de Santiago de Compostela,
15782 Santiago de Compostela, Spain
Fax: +34-981547-163
E-mail: qiac01@usc.es
[b] Departamento de Química Inorgánica, Facultad de Farmacia, Universidad de Valencia,
46100 Valencia, Spain
[c] Departamento de Química Física, Facultad de Farmacia, Universidad de Santiago de Compostela,
15782 Santiago de Compostela, Spain
[d] Departamento de Química Inorgánica, Facultad de Farmacia, Universidad de Granada,
18071 Granada, Spain
[e] Department of Chemistry, University of Washington,
Box 351700, Seattle, WA 98195-1700, USA

or polynuclear in conjunction with an additional ligand such as a halogen.

The ability of these ligands to be deprotonated in a suitable basic medium frequently leads to the formation not only of neutral mononuclear species but also polynuclear entities in which the thiosemicarbazone acts as a bridging ligand − generally through the thiolate sulfur atom.[6–8]

Although complexes of a number of metals with 2-pyridineformamide thiosemicarbazone (HAm4DH)[9–12] or its ^4N-substituted derivatives[13–21] have been studied, the coordination of these ligands with copper(II) has scarcely been investigated hitherto.[16,22,23] To explore their versatility further, in the work described here we prepared a number of copper(II) complexes of HAm4DH and determined their thermal, magnetic, and redox properties, the X-ray crystal structures of the complexes $[Cu(HAm4DH)Cl_2]_2$ (**5a**), $^1_\infty$[Cu(Am4DH)Cl] (**5b**), $^1_\infty$[Cu(Am4DH)Br] (**6a**), and $[Cu(HAm4DH)(H_2O)(ClO_4)_2]\cdot MeOH\cdot H_2O$ (**9a**), and the in vitro nuclease activities of a selection of these compounds.

Results and Discussion

The reactions between different copper(II) salts and HAm4DH, in neutral or slightly basic ethanolic media, gave a series of complexes with the general formulae $[Cu(HAm4DH)X_2]$ (X = Cl or Br) (**1**, **2**), $[Cu(HAm4DH)_2]X_2$ (X = NO_3 or ClO_4) (**3**, **4**), [Cu(Am4DH)X] (X = Cl, Br, AcO, or NO_3) (**5**–**8**), $[Cu(H_2O)(Am4DH)](ClO_4)$ (**9**), and $[Cu(Am4DH)_2]$ (**10**). These compounds generally have melting points above 200 °C and are soluble in DMF and DMSO, partially soluble in methanol, but insoluble in other commonly used organic solvents. The mass spectra of the complexes (FAB) in some cases show the molecular ion peak, although the most significant peaks correspond to the fragments $[Cu(HAm4DH)_2]^+$, $[Cu(HAm4DH)X]^+$, and $[Cu(HAm4DH)]^+$, where X is the corresponding anion. These fragmentation patterns involve the addition or loss of a hydrogen atom from the fragments.

The molar conductivities of freshly prepared solutions of the complexes in DMF are in the range Λ_m = 23–63 $S\cdot cm^2\cdot mol^{-1}$, which indicates that the compounds are neutral. However, $[Cu(Am4DH)(H_2O)](ClO_4)$ is a 1:1 electrolyte (Λ_m = 96 $S\cdot cm^2\cdot mol^{-1}$). The molar conductivity values for $[Cu(HAm4DH)_2](NO_3)_2\cdot EtOH$ and $[Cu(HAm4DH)_2](ClO_4)_2$ are 152 and 168 $S\cdot cm^2\cdot mol^{-1}$, respectively, and these values correspond to 1:2 electrolytes.[24]

Single crystals of the complexes $[Cu(HAm4DH)Cl_2]_2$ (**5a**), $^1_\infty$[Cu(Am4DH)Cl] (**5b**), $^1_\infty$[Cu(Am4DH)Br] (**6a**), and $[Cu(HAm4DH)(H_2O)(ClO_4)_2]\cdot MeOH\cdot H_2O$ (**9a**) suitable for X-ray diffraction were obtained by the slow evaporation of $[Cu(Am4DH)Cl]\cdot 0.5\,EtOH$ (**5**), $[Cu(Am4DH)Br]\cdot 0.5\,EtOH$ (**6**), or $[Cu(Am4DH)(H_2O)](ClO_4)$ (**9**) solutions in 1:1 mixtures of MeOH/CCl_4, MeOH/CH_3CN, or MeOH/CCl_4, respectively, in air at room temperature.

Crystal Structure of $[Cu(HAm4DH)Cl_2]_2$ (5a)

It can be seen from Figure 1 that **5a** is a centrosymmetric binuclear species. Each copper(II) center is bonded to a neutral HAm4DH molecule through the thione sulfur, azomethine nitrogen, and pyridinic nitrogen atoms. Three chlorine atoms are also bound to the metal − one terminal chlorine and the other two as bridges between the metal centers. This arrangement gives rise to an octahedral environment in such a way that the dimer is formed by two octahedra that share an edge consisting of the dimeric skeleton Cu(μ-Cl)$_2$Cu. The most significant bond lengths and angles are shown in Table 1.

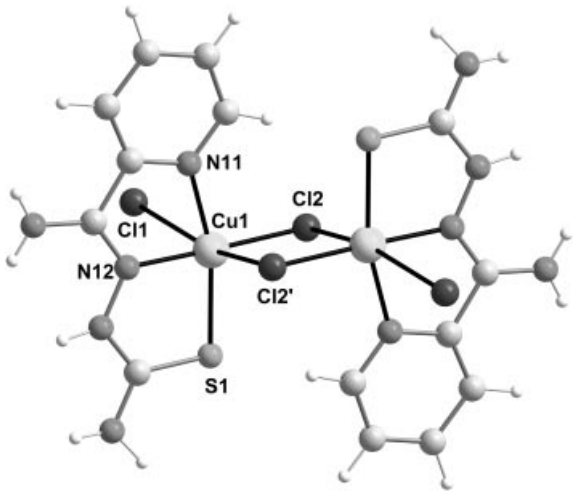

Figure 1. Perspective view of **5a** (symmetry code i: $-x + 2$, $-y$, $-z + 1$).

The formation of dimers is not unusual in copper(II) complexes of thiosemicarbazones.[4,25] However, the majority of such compounds have the formula $[Cu(L)Cl]_2$, where the bridging atom is either the sulfur or the chlorine atom, which gives rise to a coordination number of five around the metal center. In the case where L is 2-pyridinecarboxaldehyde thiosemicarbazone it was possible to obtain both structures,[4] each with a pyramidal geometry; that is, the copper(II) centers are joined either by two thiolate bridges from the thiosemicarbazone or by two chloro bridges. In contrast, compound **5a** has a coordination mode and geometry that is completely different, where the Cu(μ-Cl)$_2$-Cu skeleton has the two copper centers joined through two chloro bridges that have markedly different bond lengths: 2.219(1) Å (Cu1–Cl2^i, i: $-x + 2$, $-y$, $-z + 1$) and 3.139(1) Å (Cu1–Cl2). This gives rise to a rhomboidal geometry, with Cu–Cu and Cl–Cl distances of 3.837(1) and 3.850(2) Å, respectively, and Cl–Cu–Cl and Cu–Cl–Cu angles of 90.20(3) and 89.90(3)°, respectively. The existence of one weak and one strong Cu–Cl interaction is a characteristic feature in dimeric species with halogen bridges.[26,27] However, the second Cu–Cl distance in **5a** is at the higher limit of the sum of the van der Waals radii (3.15 Å), but is equal to or less than the order of magnitude for these bonds found in other copper(II) dimers with chloro bridges.[28] The three coordination positions around the copper center are occupied by the sulfur and two nitrogens of HAm4DH, with values of 2.027(2) and 1.941(2) Å for the Cu–Npyri-

Table 1. Selected bond lengths [Å] and angles [°] for compounds **5a**, **5b**, **6a**, and **9a**.

Compound	**5a**[a]	**5b**[b]	**6a**[c]	**9a**[d]	
Cu1–N11	2.027(2)	2.034(6)	2.034(3)	2.020(3)	2.018(3)
Cu1–N12	1.941(2)	1.934(7)	1.938(3)	1.921(3)	1.919(3)
Cu1–S1	2.296(8)	2.265(2)	2.257(1)	2.278(1)	2.277(1)
Cu1–X1	3.132(1)	2.247(2)	2.375(1)	2.498(3)	2.483(3)
Cu1–X2	3.139(1)	–	–	2.744(3)	2.852(3)
Cu1–X3	2.219(1)	2.945(2)	2.957(1)	1.964(2)	1.966(2)
Cu1–Cu1^{i}	3.837(1)	4.158(1)	4.249(1)	9.687(2)	–
N11–Cu1–N12	79.44(8)	80.0(3)	80.25(12)	80.25(11)	80.21(12)
N11–Cu1–S1	164.14(6)	164.0(2)	164.13(9)	166.21(8)	166.04(9)
N12–Cu1–S1	84.75(7)	84.3(2)	84.08(8)	85.97(9)	85.84(9)
N11–Cu1–X1	84.20(6)	97.0(2)	97.95(9)	86.6510	86.71/11)
N11–Cu1–X2	90.49(6)	–	–	81.96(11)	77.70(11)
N11–Cu1–X3	99.43(6)	86.9(2)	87.50(9)	95.41(11)	95.64(11)
N12–Cu1–X1	83.66(6)	166.3(2)	166.01(9)	92.65(11)	94.22(11)
N12–Cu1–X2	90.49(6)	–	–	86.17(12)	91.60(11)
N12–Cu1–X3	178.58(7)	98.7(2)	99.03(9)	173.76(11)	173.85(11)
S1–Cu1–X1	95.48(3)	97.6(1)	96.65(3)	94.15(7)	95.08(7)
S1–Cu1–X2	97.47(3)	–	–	97.09(9)	102.14(8)
S1–Cu1–X3	96.39(3)	98.7(1)	97.48(4)	98.33(8)	98.20(8)
X1–Cu1–X2	165.23(2)	–	–	168.58(10)	162.18(10)
X1–Cu1–X3	95.38(3)	94.5(1)	94.73(2)	91.56(10)	90.04(10)
X2–Cu1–X3	90.20(3)	–	–	88.79(12)	83.04(10)

[a] Symmetry transformation used to generate equivalent atoms i: $-x + 2, -y, -z + 1$; X3 = Cl2^{i}. [b] i: $-x - 1/2, y - 1/2, z$; X3 = Cl1^{i}. [c] i: $-x + 1/2, y - 1/2, z$; X3 = Br1^{i}. [d] X1, X2, and X3 are O11, O21, and O1 for molecule 1, and O31, O41, and O2 for molecule 2, respectively.

dine and Cu–Nazomethine, respectively, and 2.296(1) Å for the Cu–S distance. On the other hand, the Cu–Cl1 terminal distance is 3.132(1) Å, which is longer than those found in similar compounds[29,30] and is also at the higher limit of the sum of van der Waals radii (as is Cu–Cl2), a situation that confers significant ionic character to this chlorine atom.

On the basis of the information discussed above and on the assumption that each Cu is hexacoordinate, the *trans* angles N11–Cu1–S1, N12–Cu1–Cl2^{i}, and Cl1–Cu1–Cl2 [164.1(1), 178.6(1), and 165.2(1)°, respectively] and the distances discussed above suggest that each metal center has an octahedral coordination geometry with a growing tetragonal distortion of the 4+2 type, and a $CuCl_3N_2S$ chromophore in which the equatorial plane defined by the atoms S1, N12, N11, and Cl2^{i} contains the copper(II) centers (Table 2). This plane forms a dihedral angle of 1.8(1)° with the average plane corresponding to the thiosemicarbazone chain, which in turn forms an angle of 6.0° with the pyridine ring. This situation confirms that the HAm4DH ligand is almost planar in the coordination arrangement.

The bonding parameters for the thiosemicarbazone in the complex are close to those in the free ligand − apart from the N13–N12–C16 angle, which increases from 116.7(2)° to 120.1(2)° as a consequence of the involvement of N12 in coordination with the copper center.

In the crystal packing the dimeric units interact with one another through Cl1, which participates in hydrogen bonding to form chains along the [100] direction, as shown in Figure 2. Each dimeric unit is bonded to its neighbor

Table 2. Best least-squares planes for **5a**, **5b**, **6a**, and **9a**.[a]

Compound	Plane	Rms deviation [Å]	Largest deviation [Å]	Angle with previous plane [°]
5a	N11/N12/S1/Cl2^{i}	0.0192	N12, 0.023(1)	
	C16/N12/N13/C17/S1/N14	0.0183	N12, 0.036(2)	1.8(1)
	N11/C11/C12/C13/C14/C15	0.0050	C15, 0.007(2)	6.0(2)
5b	N11/N12/S1/Cl1	0.0738	N12, 0.088(3)	
	C16/N12/N13/C17/S1/N14	0.0252	N13, 0.039(6)	10.1(2)
	N11/C11/C12/C13/C14/C15	0.0075	C11, 0.013(6)	4.5(3)
6a	N11/N12/S1/Br1	0.0855	N12, 0.104(2)	
	C16/N12/N13/C17/S1/N14	0.0125	C17, 0.016(2)	9.4(1)
	N11/C11/C12/C13/C14/C15	0.0041	C13, 0.007(4)	3.3(2)
9a	N11/C11/C12/C13/C14/C15	0.0045	C15, 0.007(2)	
	C16/N12/N13/C17/S1/N14	0.0227	N12, 0.041(2)	4.5(2)
	N11/N12/S1/O1	0.0318	N12, 0.036(1)	2.4(1)
	N21/N22/S2/O2	0.0267	N22, 0.001(1)	1.1(1)
	C26/N22/N23/C27/S2/N24	0.0254	N23, 0.026(3)	2.6(11)
	N21/C21/C22/C23/C24/C25	0.0034	C22, 0.005(3)	5.7(2)

[a] Symmetry transformation used to generate equivalent atoms, i: $-x + 2, -y, -z + 1$.

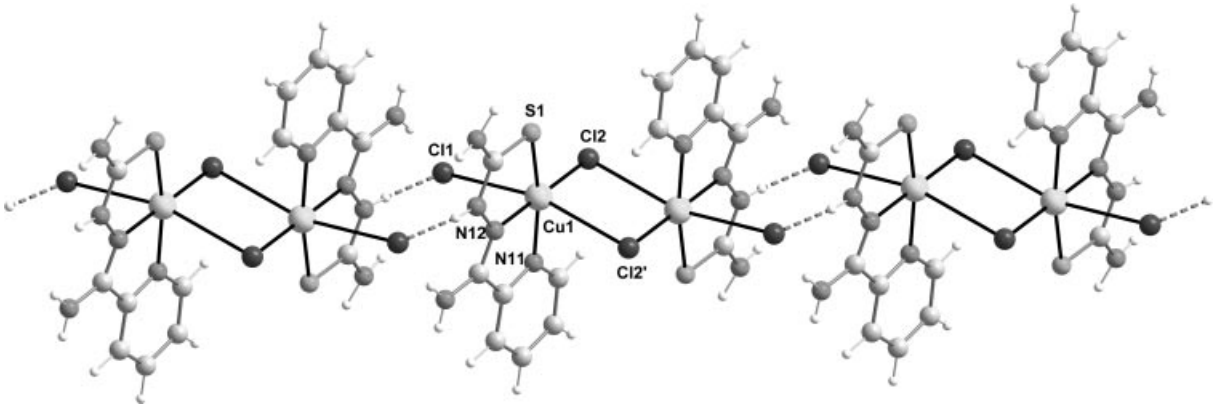

Figure 2. View of the chain structure in the crystal lattice of complex **5a**. The Cl1 atoms are responsible for linking each dimer unit to another through hydrogen bonding along the [100] direction.

through a N13–H13···Cl1^{i} bond (Table 3). The same atom acts as a hydrogen-bond acceptor with the NH_2 groups of the thiosemicarbazones from contiguous chains acting as donors. These interactions give rise to parallel layers along the *bc* plane that stack in the [100] direction.

Crystal Structure of $^{1}_{\infty}$[Cu(Am4DH)Cl] (5b) and $^{1}_{\infty}$[Cu(Am4DH)Br] (6a)

Compounds **5b** and **6a** are isotypic and their structures are formed by chains along the *a* axis. Each copper(II) cen-

Table 3. Hydrogen bonding interactions for **5a**, **5b**, **6a**, and **9a**.

Compound	D–H···A	*d*(D–H)	*d*(H···A)	*d*(D···A)	∠(DHA)
5a[a]	N13–H13···Cl1^{1}	0.89	2.19	3.078(2)	174.7
	N14–H14A···Cl1^{1}	0.89	2.88	3.603(3)	139.6
	N14–H14B···Cl1^{2}	0.95	2.86	3.328(2)	111.9
	N14–H14B···Cl2^{3}	0.95	2.95	3.670(3)	133.3
	N15–H15A···Cl1^{1}	0.87	2.52	3.377(2)	173.3
	N15–H15B···Cl1^{4}	0.83	2.48	3.274(2)	161.6
5b[b]	N14–H14A···N13^{1}	0.96	2.15	3.090(10)	165.9
	N14–H14B···S1^{2}	0.97	2.55	3.510(7)	167.6
	N15–H15B···Cl1^{3}	0.86	2.63	3.44(7)	159.2
6a[c]	N14–H14A···S1^{1}	0.81	2.69	3.503(4)	173.7
	N14–H14B···N13^{2}	0.85	2.22	3.074(5)	174.8
	N15–H15B···Br1^{3}	0.84	2.68	3.468(3)	157.0
9a[d]	O1–H1B···O33^{1}	0.77	2.11	2.862(4)	168.3
	O1–H1B···O13	0.77	2.62	3.077(4)	119.4
	N13–H13A···O5	0.97	1.76	2.723(5)	168.2
	N14–H14A···O32^{2}	0.88	2.09	2.942(4)	162.7
	N14–H14B···O34^{3}	0.90	2.20	3.011(4)	151.0
	N15–H15A···O5	0.84	2.27	3.078(4)	163.4
	N15–H15B···O3	0.90	2.04	2.894(4)	157.9
	O2–H2A···O3	0.87	1.85	2.710(4)	173.4
	O2–H2B···O13^{1}	0.78	2.12	2.864(4)	161.0
	O2–H2B···O33	0.78	2.53	3.065(4)	126.8
	N23–H23A···O6^{4}	0.92	1.83	2.744(4)	175.4
	N24–H24A···O12^{4}	0.83	2.15	2.950(4)	164.2
	N24–H24B···O14^{3}	0.91	2.18	3.028(4)	154.9
	N25–H25A···O6^{4}	0.81	2.31	3.064(4)	155.0
	N25–H25B···O4^{5}	0.87	2.08	2.907(4)	157.9
	O5–H5A···O43^{6}	0.88	2.15	2.964(5)	154.1
	O6–H6A···O14^{1}	0.95	2.19	3.038(4)	149.4
	O3–H3A···O41	0.87	2.23	2.830(4)	126.2
	O3–H3A···O42^{6}	0.87	2.39	3.072(4)	135.4
	O3–H3B···O22^{7}	0.76	2.11	2.810(5)	153.9
	O4–H4A···O21^{1}	0.90	2.30	2.958(5)	129.7
	O4–H4A···O24^{8}	0.90	2.38	3.025(4)	128.0
	O4–H4B···O43^{9}	0.80	2.11	2.786(4)	141.8

[a] Symmetry transformations used to generate equivalent atoms: **1**: $-x + 1, -y, -z + 1$; **2**: $x, -y - 1/2, z + 1/2$; **3**: $-x + 2, y - 1/2, -z + 3/2$; **4**: $x, -y + 1/2, z + 1/2$. [b] **1**: $-x, y, -z + 1/2$; **2**: $-x, -y, -z + 1$; **3**: $-x - 1/2, -y - 1/2, z - 1/2$. [c] **1**: $-x, -y + 1, -z + 1$; **2**: $-x, y, -z + 1/2$; **3**: $-x + 1/2, -y - 1/2, z - 1/2$. [d] **1**: $-x + 1, -y + 1, -z + 1$; **2**: $x, y, z + 1$; **3**: $-x, -y + 1, -z + 1$; **4**: $x - 1, y, z$, **5**: $-x, -y + 1, -z$; **6**: $-x, -y, -z + 1$; **7**: $-x + 1, -y, -z + 1$; **8**: $x, y + 1, z + 1$; **9**: $x, y + 1, z$.

ter is coordinated to a deprotonated thiosemicarbazone through the thiolate sulfur atom and the azomethine and pyridine nitrogen atoms, a situation that is common with this type of ligand. The structure of the 1D coordination polymers is formed by the asymmetric halogen bridges between the metal centers, which gives rise to pentacoordination around each copper(II) center (Figure 3). In both complexes the Cu–S, Cu–Nazomethine, and Cu–Npyridine distances (Table 1) are very similar and the most marked difference (0.008 Å) is in the Cu–S bond of **5b**. This in turn is associated with the largest deviation (0.039 Å), which is not particularly significant in comparison with that in **5a**.

The Cu–Cl distances in **5b** are 2.247(2) and 2.945(2) Å and, although these are significantly different, they are more similar to one another than those found in the dimer **5a** (differences of 0.920 Å vs 0.694 Å). The shortest distance is slightly longer than those found in other copper(II) complexes with thiosemicarbazone ligands and chloro bridges[25] and the longest distance is in the range found in other systems with chloro bridges between copper centers (2.70–3.19 Å).[31,32]

In **6a** both Cu–Br bond lengths are also significantly different. However, in this case the difference is 0.582 Å, which represents the smallest difference of the three complexes under discussion. However, the bond lengths are shorter and longer, respectively, than those found in $[Cu(dmamhp)Br_2]_2$ (dmamhp = 2-dimethylaminomethyl-3-hydroxypyridine), a dimer that contains asymmetric bromo bridges with Cu–Br distances of 2.439(2) and 2.805(2) Å.[33]

The τ values found in the two complexes[34] are 0.039 for **5b** and 0.031 for **6a**, and these are consistent with the copper(II) atoms having a tetragonal pyramidal coordination environment ($\tau = 0$) with a distortion towards trigonal bipyramidal ($\tau = 1$). In this arrangement the basal plane is defined by N11, N12, S1, and X1, all of which are coplanar [maximum deviations of 0.088(3) and 0.104(2) Å in N12 for **5b** and **6a**, respectively], and the copper center is located 0.170(3) Å above this plane in **5b** and 0.173(1) Å above it in **6a** (Table 2). This basal plane forms angles of 10.1(2) and 9.4(1)° with the plane of the thiosemicarbazone chain, which in turn forms angles of 4.5(3) and 3.3(2)°, respectively, with the best least-squares plane of the pyridine ring.

The axial position is occupied by the neighboring halogen atom that forms the bridge (symmetry code: $-x - 1/2$, $y - 1/2$, z) and this gives rise to angles in the range 86.9(2)–98.7(1) Å in **5b** and 87.5(1)–99.0(1) Å in **6a** (Table 1). The chains develop along the [010] direction and in these chains the Cu···Cu separations are 4.158(1) and 4.249(1) Å for **5b** and **6a**, respectively. This level of separation is sufficiently large that magnetic interactions can take place between the metal centers.

In contrast to the situation in **5a**, a number of significant changes are apparent in **5b** and **6a** in terms of the bonding parameters of HAm4DH when compared to the data for the free ligand. These changes are due to deprotonation of the ligand and mainly affect the bond lengths and angles around C17. This situation gives rise to elongation of the S1–C17 and N14–C17 bonds from average values of 1.698(2) and 1.316(3) Å to 1.741(6) and 1.363(6) Å, respectively. On the other hand, the N13–C17 bond decreases in length from 1.340(2) to 1.305(8) Å. Some bond angles also experience significant changes on complexation and this is due to the presence of the thiolate form of the ligand; S1–C17–N14 and C17–N13–N12 are modified from average values of 123.0(2) and 118.3(2)° in HAm4DH to 116.8(5) and 111.3(5)°, respectively, while S1–C17–N13 changes form 120.3(2) to 125.4(5)°. These changes are clearly a result of changes in the electronic delocalization in the thiosemicarbazone chain on conversion to the thiol form of the ligand and subsequent deprotonation in the basic medium.

A number of hydrogen bonds are formed in the crystal packing arrangement. The most significant of these occur between the amino donor groups and the imine nitrogen atoms of neighboring chains, which act as acceptors (Table 3). These interactions give rise to a three-dimensional supramolecular network.

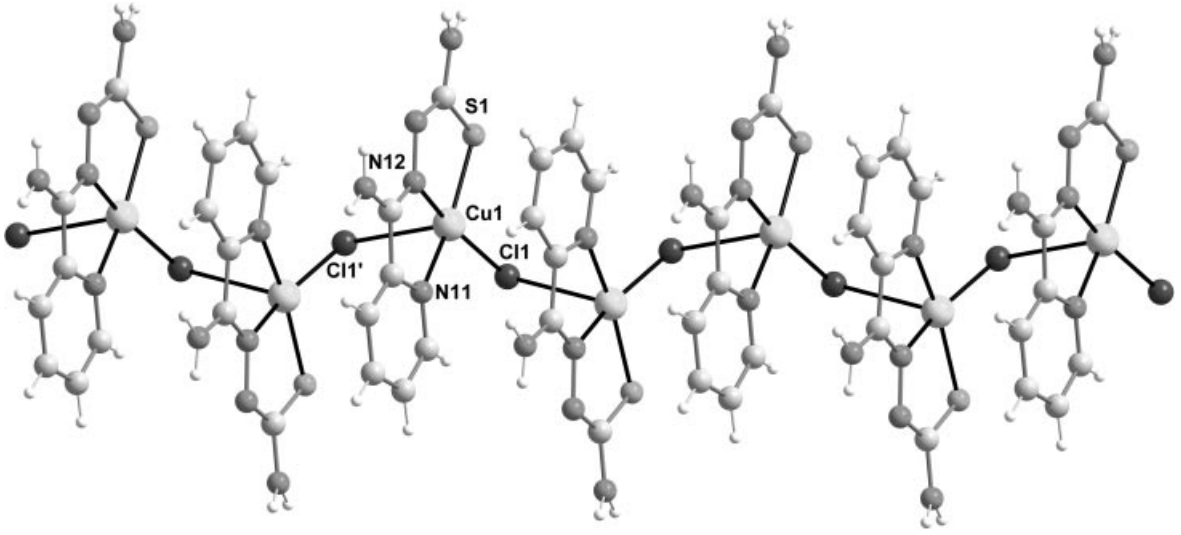

Figure 3. Perspective view of the 1D-chain structure of **5b** along the *b* axis.

Crystal Structure of $[Cu(HAm4DH)(H_2O)(ClO_4)_2]\cdot MeOH\cdot H_2O$ (9a)

The asymmetric unit consists of two complex molecules that are crystallographically independent (I and II), and are separated by a Cu···Cu distance of 9.687(2) Å. In each molecule the copper(II) center is hexacoordinate by a neutral thiosemicarbazone molecule through the sulfur atoms and the usual nitrogen atoms, an oxygen atom from a water molecule, which occupies the equatorial positions, and two oxygen atoms from the perchlorate ligands, which occupy the axial positions. Figure 4 is a diagram of molecule I.

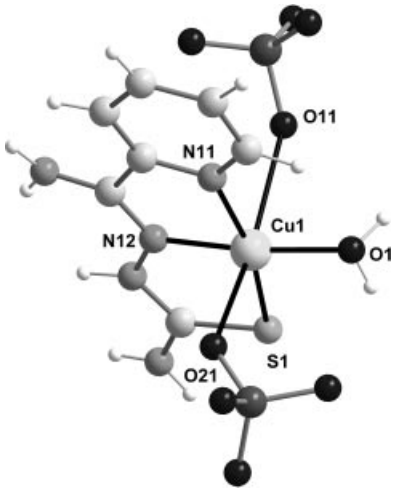

Figure 4. Representation of molecule I of **9a**.

In the equatorial plane the metal–ligand distances in the two molecules range from 1.919(3) Å for the Cu–Nazomethine distance in the second molecule to 2.278(1) Å for the Cu–S distance in the first molecule (Table 1). The axial Cu–O distances are different and this gives rise to a 4+1+1 distortion in the coordination polyhedron. One of the Cu–O distances is around 2.5 Å and the other around 2.8 Å. These distances are considerably longer than the equatorial Cu–Owater distance, which has an average value of 1.965(2) Å, but are of the same order of magnitude as those found in other copper(II) complexes with coordinated perchlorate groups.[5,26,35–37]

Another indication of the magnitude of the distortion is given by the *trans* angles in the equatorial plane, which have average values of 166.1(1)° for N11–Cu1–S1 and 173.8(1) for N12–Cu1–O1. However, the clearest evidence of distortion is provided by the *trans* angle between the axial positions, with values of 168.6(1)° in the first molecule and 162.2(1)° in the second. These bond angle values are comparable to those found in other copper(II) complexes with coordinated perchlorate ligands but are larger than the value of 155.9(2)° found in $[Cu(HL)(H_2O)(ClO_4)_2]$, where HL is 2-formylpyridine thiosemicarbazone.[5] In both molecules the equatorial plane containing each Cu atom is approximately coplanar with the corresponding thiosemicarbazone plane [dihedral angles are 2.4(1) and 2.6(1)°] (Table 2), which in turn form angles of 4.5(2) and 5.7(2)° with the best least-squares plane of the pyridine ring.

Once again in this complex − as in the case of **5a** − only the N13–N12–C16 angle changes and this angle has values of 120.7(3) and 120.2(3)° in the two molecules in the complex.

Numerous hydrogen-bonding interactions occur in the crystal packing arrangement (Table 3) and it is not only the amine and imine groups of HAm4DH that take part but also the water and ethanol molecules and the noncoordinated oxygen atoms of the perchlorate ligands.

Spectral Studies

The IR spectra of the Cu^{II} complexes contain bands in the range 3473–3158 cm^{-1} and these correspond to ν(NH) and, in cases where the complex contains solvent molecules, ν(OH). Bands are also observed between 1610 and 1568 cm^{-1} and these are due to ν(CN+CC).

The C=S vibration modes are seen for the ligand HAm4DH at 853 cm^{-1} and this band is observed at lower frequencies in the complexes, which shows that coordination of the thio donor to the copper center has taken place. In the free ligand the band corresponding to ν(NN) is observed at 999 cm^{-1}, while in all of the complexes this band appears at higher frequencies because of coordination of the metal center through the sulfur and azomethine nitrogen atom.

The diffuse reflectance spectra of all of the complexes show three broad bands in the visible region. The intense band, which has the high energy, appears at 26350–26724 cm^{-1} and has a shoulder on the highest energy side. This band is due to ligand transitions: $n \rightarrow \pi^*$ (main band) and $\pi \rightarrow \pi^*$ (shoulder). A second band is observed between 22624 and 24232 cm^{-1} and this has various components that must correspond to metal–ligand charge-transfer processes (MLCT), probably $\sigma(S) \rightarrow d_{x^2-y^2}$ (Cu^{II}) or $\pi \rightarrow d_{x^2-y^2}$ (Cu^{II}). In contrast to other copper(II) complexes, in this case there does not seem to be a clear correlation between the position of the maximum of this band and the coordination geometry or the nature of the ligand coordinated to the metal. The band that is observed in the lower energy region of the spectrum has two components at 15244–16353 and 14245–15785 cm^{-1} and these correspond to a d–d transition.[38]

The EPR spectra of polycrystalline samples, measured at room temperature, are axial and isotropic. The spectra of complexes **1** and **8** are practically identical and show an axial nature (Figure 5, a) and very similar EPR parameters for the two complexes, a situation that suggests the same coordination polyhedron around copper(II). Given that $g_{\|} > g_{\perp}$, the unpaired electron is located in a $d_{x^2-y^2}$ orbital and this is characteristic of a distorted tetragonal structure. Complex **7** gives rise to an axial spectrum that is slightly rhombic, as can be seen in Figure 5 (b). The EPR parameters of this complex are practically identical to those of the two complexes discussed above. The complexes are also quasi-isotropic.

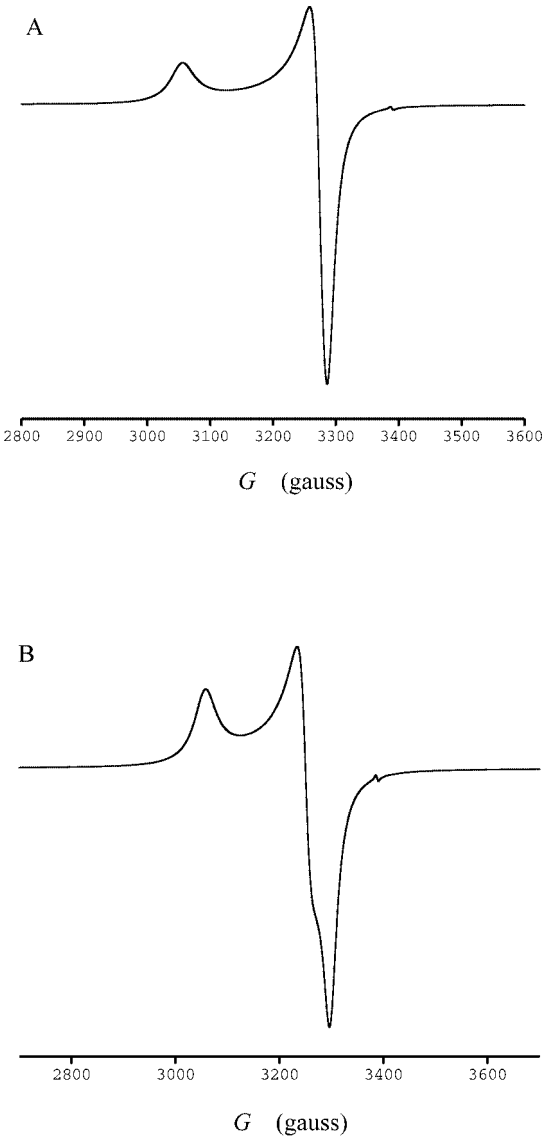

Figure 5. ESR spectra of **1** (A) and **7** (B) at room temperature.

Magnetic Behavior

The magnetic moments of the complexes were measured at room temperature (298 K) and the majority are in the range 1.75–2.20 BM, which is characteristic of mononuclear copper(II) complexes. However, in compound **5a**, $[Cu(HAm4DH)Cl_2]_2$, the value is 1.24 BM and this is lower than the expected spin-only value, which clearly indicates antiferromagnetic coupling between the copper(II) ions. This behavior is very similar to that found in binuclear copper(II) complexes containing chloro bridges. In order to determine the extent of the magnetic interaction between the two metal ions and to elucidate the difference in the singlet–triplet energy values, the magnetic susceptibility was measured in the temperature range 2–150 K. The variation in the magnetic susceptibility with temperature is shown in Figure 6. It can be seen that the magnetic susceptibility increases to a maximum at 15 K on cooling and then falls rapidly on decreasing the temperature further. The experimental magnetic susceptibility values (corrected for diamagnetism) were adjusted using the Bleaney–Bowers equation[39] for a coupled dinuclear copper(II) species:

$$\chi_M = \{(Ng^2\beta^2)/kT[3 + \exp(-J/kT)]\}^{-1}(1 - \rho) + \rho Ng^2\beta^2/4kT + \chi_{TIP}$$

which results from considering the same values of $H = -2JS_1S_2$ and where the symbols have the accepted meanings. A nonlinear least-squares adjustment program was used to calculate $-J$ and g and excellent agreement was obtained when $J = -12.2$ cm^{-1}, $g = 2.17$, $\chi_{TIP} = 124\times10^{-6}$, $\rho = 0.035$, and $R = 1.2\times10^{-3}$. The coupling constant calculated for the singlet–triplet exchange clearly shows that antiferromagnetic interactions exist between the copper(II) ions in **5a** in the solid phase.

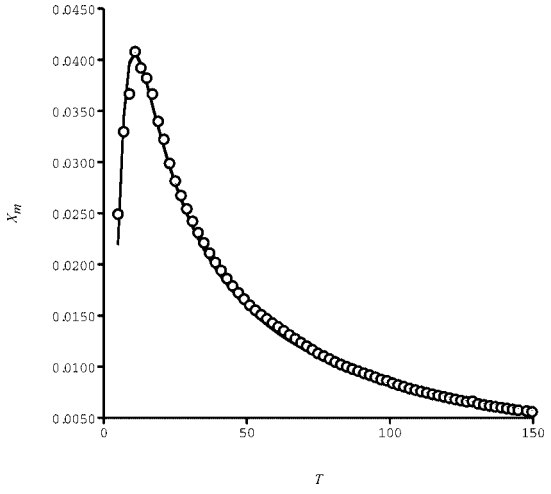

Figure 6. Temperature [K] dependence of the magnetic susceptibility χ_M (cm^3·mol^{-1}) of **5a**. The solid line represents the least-squares fit equation and the parameters described in the text.

In contrast to copper(II) complexes containing hydroxy bridges, which have equivalent Cu–O (bridge) distances, dimers with chloro bridges frequently have different Cu–Cl (bridge) distances and the singlet–triplet splitting depends on the length of the bridging bonds and the Cu–Cl–Cu angle of the bridge.[40]

Correlation studies were carried out on the magnetic and structural properties of a diverse range of dinuclear copper(II) species − particularly compounds with two chloro bridges between the metal centers and trigonal pyramidal or square-pyramidal coordination geometries. Reasonable consistency was found in that the singlet–triplet splitting and, consequently, the isotropic interaction parameter ($2J$) correlate reasonably well with the φ/r ratio between the bridging angle Cu–Cl–Cu′ (φ) and the longest Cu–Cl distance from the basal plane (r). The φ/r values between 32.5 and 34.75 °/Å correspond to ferromagnetic interaction while values outside this range correspond to antiferromagnetic behavior.[41] The φ/r value found for compound **5a** is 28.6 °/Å and this is consistent with the correlation.

However, this situation contrasts with that found for $[(dpt)Cu(\mu\text{-}Cl)_2Cu(dpt)]Cl_2$ (dpt = dipropylenetriamine, φ/r

= 35.9 °/Å), where each copper(II) ion is in a trigonal bipyramidal environment and the compound shows ferromagnetic coupling between the copper(II) ions (J = 42.9 cm^{-1}) and an interdimeric antiferromagnetic coupling (J' = –3.92 cm^{-1}).[42] Another similar example is [(depc)(Cl)Cu(μ-$Cl)_2$Cu(Cl)(depc)] (depc = diethyl pyridine-2,6-dicarboxylate, φ/r = 40.9 °/Å), in which each copper(II) ion is in a distorted octahedral environment and coupling constants of J = 39.9 cm^{-1} and J' = –0.59 cm^{-1} are found.[43]

Thermochemistry

The pyrolysis of the compounds subjected to thermogravimetric analysis (**1**–**3**, **5**–**8**, **10**) occurred in four or five stages, with overall evolution of H_2O, CO_2, CO, NH_3, NO, NO_2, and SO_2 in all cases except that of compound **7**, for which only three stages and the evolution of only H_2O, CO_2, NO, NO_2, and SO_2 were detected (Table 4). In keeping with their observed crystal structures, compounds **1** and **7** gave off no solvent molecules, and these compounds were stable up to 226 °C and 174 °C, respectively. The remaining compounds, which are all solvated, lost solvent molecules even at room temperature, because of which the number of solvent molecules included in the working empirical formula of the starting material was calculated as that which gave the best agreement with the experimental weight loss during the first decomposition stage, assuming this stage to involve only solvent loss; for example, for compounds **3** and **10** this procedure afforded the working empirical formulae $[Cu(HAm4DH)_2](NO_3)_2 \cdot 0.52\,EtOH$ and $[Cu(Am4DH)_2] \cdot 1.27\,H_2O$, respectively. Note that the final residue of compound **7**, the only compound not to give off ammonia as well as SO_2 and nitrogen oxides, was $Cu(NO_3)_2$, and that for all compounds except compound **7** the final residue accounted for a greater percentage of the initial mass than would correspond to its consisting entirely of CuO, the difference being quite substantial in some cases; this suggests that in these cases, too, the residue may have contained $Cu(NO_3)_2$, or perhaps a copper(II) oxy-nitrate, even though only CuO was detected.

Cyclic Voltammetry Studies

The reduction peak potentials for Cu^{II} are shown in Table 5 along with the corresponding reoxidation peaks for Cu^{I}. It can be seen that the more negative the cathodic peak, the more stable the complex (for a variation in potential of 0.02 $V \cdot s^{-1}$).

Table 5. Reduction peak potentials for Cu^{II} and the corresponding peaks for the reoxidation of Cu^{I}.

	V = 0.02 $V \cdot s^{-1}$			V = 0.2 $V \cdot s^{-1}$		
	E_c[a]	E_a[a]	$E_c - E_a$[a]	E_c[a]	E_a[a]	$E_c - E_a$[a]
1	–0.532	–0.379	–0.135	–0.597	–0.413	–0.184
2	–0.572	–	–	–0.662	–0.121	–0.541
3	–0.562	–	–	–0.655	–0.192	–0.463
4	–0.406	–	–	–0.452	–	–
5	–0.564	–0.425	–0.139	–0.610	–0.345	–0.265
6	–0.501	–0.384	–0.117	–0.523	–0.307	–0.216
7	–0.493	–0.326	–0.167	–0.544	–0.292	–0.252
8	–0.432	–	–	–0.465	–	–
9	–0.610	–0.054	–0.556	–0.685	0.052	–0.737
10	–0.663	–0.375	–0.288	–0.618	–0.224	–0.394

[a] V vs. SCE.

In all cases a well-defined cathodic peak was observed and, based on the position of the peak on the potential scale (–0.4 to –0.8 V vs SCE) and its absence in the reverse measurements on the ligands, this can be attributed to the reduction of copper(II) according to the equation:

$$Cu^{2+} + e^- \leftrightarrows Cu^+$$

In the majority of the complexes the corresponding anodic peak is also observed (E_a) (Figure 7), although in some cases the appearance of the peak depends on the experimental conditions (e.g. potential range and length of time after preparation of the solution). The peak shapes and the separation between the cathodic and anodic peaks (when they are observed) demonstrate the irreversible nature of the electrode process.

Voltammograms were also obtained over a larger potential range and these showed a cathodic peak at around –2 V versus SCE, which is also present in the voltammograms obtained for the ligand (Figure 8). This peak can be assigned to reduction of the ligand from the thione to the thiol, as proposed by other authors for similar conditions.[44] An anodic peak was also observed in the potential range 0.5–0.6 V versus SCE (Figure 9) and the origin of this peak is not clear because of its changeable behavior.

In complexes **3**, **8**, **9**, and **10** the peak due to the reduction of copper(II) is split into two very close peaks that

Table 4. Data for the thermogravimetric analysis of Cu^{II}.

	Stages	% Total	ΔT [°C]	Gases evolved in stage 1	Gases evolved in other stages	Final residue (% exp. – % calcd.)
1	4	70.85	226–524	H_2O, CO_2, CO, NH_3, NO_2	H_2O, CO_2, CO, NH_3, N_2O, NO, NO_2, SO_2	CuO (29.15–24.13)
2	5	76.04	r.t.–737	H_2O, CO_2	H_2O, CO_2, CO, NH_3, N_2O, NO, NO_2, SO_2	CuO (23.96–17.65)
3	5	74.86	r.t.–511	H_2O, CO_2	H_2O, CO_2, CO, NH_3, N_2O, NO, NO_2, SO_2	CuO (33.65–25.11)
5	4	71.42	r.t.–512	H_2O, CO_2, NO_2	H_2O, CO_2, CO, NH_3, N_2O, NO, NO_2, SO_2	CuO (28.58–25.15)
6	5	76.87	r.t.–773	H_2O, CO_2, NO_2	H_2O, CO_2, CO, NH_3, N_2O, NO, NO_2, SO_2	CuO (23.13–22.05)
7	3	66.35	174–474	H_2O, CO_2, NO	H_2O, CO_2, NO_2, SO_2	$Cu(NO_3)_2$ (27.57–29.21)
8	4	65.76	r.t.–526	H_2O, CO_2, CO, NH_3, NO_2	H_2O, CO_2, CO, NH_3, N_2O, NO, NO_2, SO_2	CuO (34.24–18.54)
10	5	73.86	r.t.–524	H_2O, CO_2, CO, NH_3	H_2O, CO_2, CO, NH_3, N_2O, NO, NO_2, SO_2	CuO (26.14–15.18)

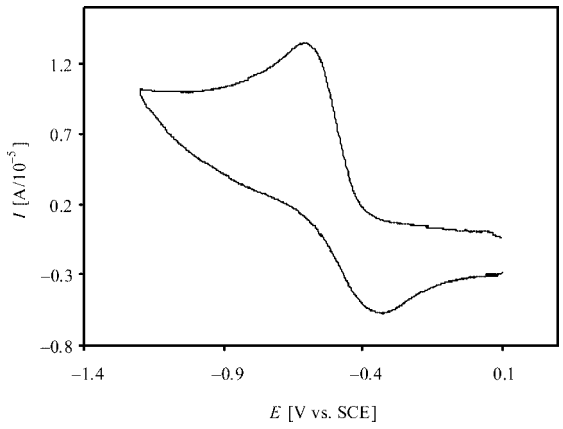

Figure 7. Cyclic voltammogram of complex **5** in 10^{-3} M DMF (scan rate 0.2 V·s^{-1}).

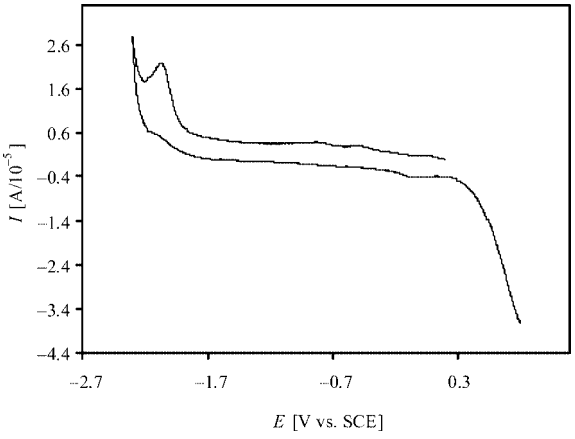

Figure 8. Cyclic voltammogram (scan rate 0.2 V·s^{-1}) of a 1 mM solution in DMF of HAm4DH.

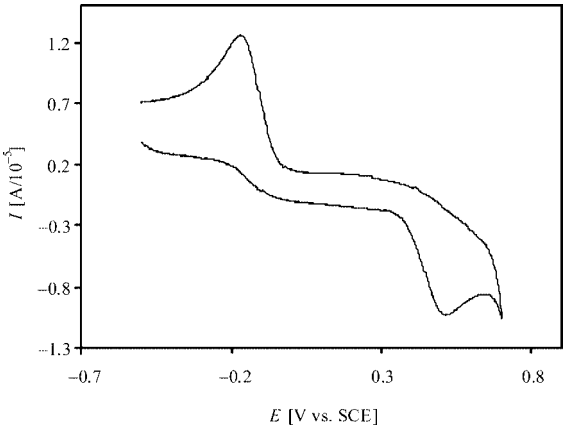

Figure 9. Cyclic voltammogram (scan rate 0.2 V·s^{-1}) of a 1 mM solution in DMF of **1**.

practically overlap (Figure 10) − these peaks are due to the presence of two chemically very similar species in solution. In the case of complex **9** this splitting becomes more marked as the length of time after preparation of the solution increases. This change indicates a progressive change in the structure of the ligand. Complexes **1** and **7** also show splitting of the cathodic peak because of the reduction of copper(II) (Figure 11) but, given the characteristic shape of one of the peaks, this splitting can be attributed to the fact that a proportion of the electrochemical reaction takes place at the surface.

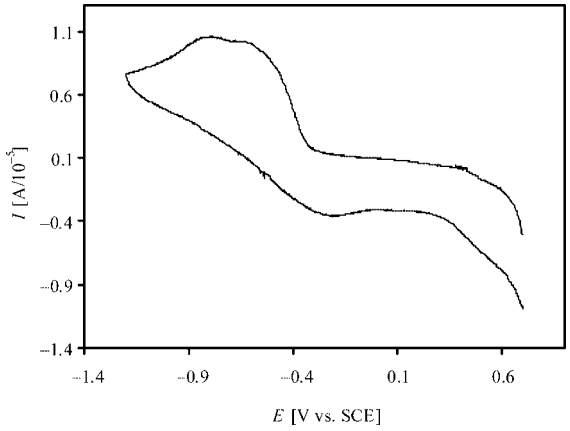

Figure 10. Cyclic voltammogram of complex **10** in 10^{-3} M DMF (scan rate 0.2 V·s^{-1}).

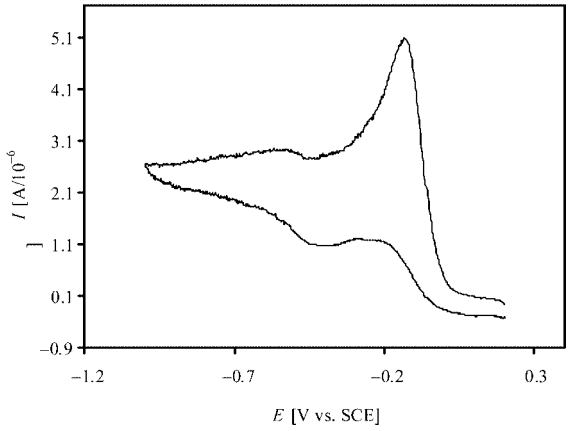

Figure 11. Cyclic voltammogram of complex **1** in 10^{-3} M DMF (scan rate 0.2 V·s^{-1}).

Similar splitting − albeit less marked − was observed in the anodic peak associated with the reoxidation of copper(I).

The Activity of Thiosemicarbazone/Copper Complexes as DNA Nucleases

The electrophoresis studies carried out on complexes **1**, **2**, **5**, and **6** (Figure 12) show that these materials have nuclease activity because a significant proportion of the DNA, which is initially supercoiled (lane 2), appears in a circular form when incubated in the presence of 12 μM of complex (lanes 5, 7, 9, and 11, respectively). It can also be seen that the nuclease capacity of the four complexes under investigation is dependent on the concentration, as the digestion observed on incubating the DNA with 24 μM of the complex is higher than that produced with 12 μM for all four complexes.

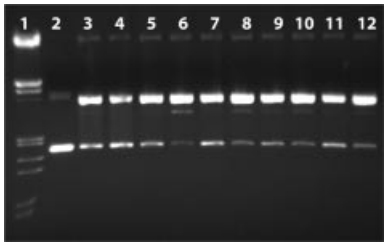

Figure 12. Agarose gel electrophoresis of pUC18 plasmid DNA treated with complexes **1**, **2**, **5** and **6** or $CuSO_4$ in the presence of 50 equiv. H_2O_2/ascorbate tandem. Incubation time 1 h (37 °C). Lane 1, λDNA/EcoR1 + HindIII Marker; lane 2, supercoiled DNA (control); lane 3, $Cu(SO_4)$ 40 μM; lane 4, $Cu(SO_4)$ 80 μM; lane 5, complex **2** 12 μM; lane 6, complex **2** 24 μM; lane 7, complex **6** 12 μM; lane 8, complex **6** 24 μM; lane 9, complex **1** 12 μM; lane 10, complex **1** 24 μM; lane 11, complex **5** 12 μM; lane 12, complex **5** 24 μM. Incubation time 1 h (37 °C).

It is known that copper has nuclease activity in its own right and, for this reason, the digestion produced by $CuSO_4$ under the same conditions was also determined. It can be seen from Figure 12 that the presence of $CuSO_4$ causes a proportion of the DNA to change to the circular form upon digestion (lanes 3 and 4). Complexes **1**, **5**, and **6** show practically identical nuclease activity to that shown by copper under the same conditions (cf. lanes 3–4 with 7–8, 9–10 and 11–12). The activity of these complexes must therefore be due to the presence of copper. In contrast, at a concentration of 24 μM complex **2** causes complete digestion of the supercoiled plasmid to give the circular form and a small quantity of the linear form. This complex clearly shows higher activity than $CuSO_4$ under the same experimental conditions (lanes 4 and 6).

In an effort to determine the mode of action of the nuclease process associated with complex **2**, we assessed the influence of different agents that could potentially inhibit reactive oxygen species (ROS). These compounds included hydroxy radical scavengers (DMSO and *tert*-butyl alcohol), singlet oxygen scavengers (sodium azide and 2,2,6,6-tetramethyl-4-piperidone), and superoxide radical scavengers (SOD). Finally, distamycin was tested as a species that bonds to DNA in the minor groove. Comparison of lanes 4 and 5 (Figure 13), which represent assays with DMSO and *tert*-butyl alcohol, respectively, with lane 3 (absence of inhibitor) shows that these additives do inhibit the process. This observation indicates the participation of the hydroxy radical in the DNA digestion process. Sodium azide (lane 6) and 2,2,6,6-tetramethyl-4-piperidone (lane 7) also inhibit the nuclease activity of the complex. This finding shows that singlet oxygen − or a species that behaves in a similar way − is also involved in the nuclease process. It is worth highlighting that azide can form complexes with copper and in this case the inhibition is markedly higher than that observed with 2,2,6,6-tertramethyl-4-piperidone. The presence of distamycin in the reaction mixture did not lead to changes in the activation of the complex, as can be seen in lane 8. This observation shows that the complex does not interact with DNA through the minor groove. The SOD enzyme, on the other hand, increased the nuclease activity and lane 9 shows total degradation of the plasmid. The dismutation process of the superoxide ion probably gives rise to a greater proportion of hydroxy radicals, which are produced by decomposition of hydrogen peroxide produced in the dismutation process.

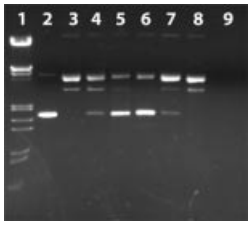

Figure 13. Agarose gel electrophoresis of pUC18 plasmid DNA treated with 24 μM of complex **2** and different inhibitors in the presence of H_2O_2/ascorbate (50 times more concentrated than the complex). Incubation time 1 h (37 °C). Lane 1, λDNA/EcoR1 + HindIII Marker; lane 2, supercoiled DNA (control); lane 3, complex without inhibitor; lane 4, complex + 1 M DMSO; lane 5, complex + 1 M *tert*-butyl alcohol; lane 6, complex + NaN_3 (100 mM); lane 7, complex + 2,2,6,6-tetramethyl-4-piperidone (100 mM); lane 8, complex + distamycin (8 μM); lane 9, complex + SOD (15 units).

These results imply that the $OH^{\cdot}$ radicals take part in the nucleic acid digestion process in the same way as singlet oxygen (or a species with similar behavior). The following mechanism can be proposed for the process:

1. reduction of Cu^{II} to Cu^{I};
2. interaction of the Cu^{I} complex with DNA, possibly through the major groove;
3. reaction between hydrogen peroxide or oxygen with the Cu^{I} to form the reactive oxygen species;
4. reaction of the hydroxy radical and singlet oxygen with DNA and destruction of the strands.

If the reactive species are not generated in the immediate vicinity of the DNA they can diffuse and be neutralized. For this reason the structures of the complexes and the nature of the ligand govern the DNA recognition process and determine the level of chemical damage.

The fact that the complex does not intercalate with the minor groove of the double helix possibly means that the reduction of Cu^{II} to Cu^{I} and the production of reactive oxygen species capable of attacking the DNA do not take place in the vicinity of the DNA. For this reason the digestion process is not as effective as that in cases where the complexes act by intercalation, for example, $[Cu(phen)_2]^{2+}$. This could be the reason why complex **2** shows a higher nuclease activity than the other compounds synthesized in this study.

Experimental Section

General: Elemental analyses were carried out with a Carlo–Erba Model 1108 and Perkin–Elmer 240B microanalyzer. IR spectra were recorded with a Bruker IFS-66 V spectrophotometer as KBr disks (4000–400 cm^{-1}) or polyethylene-sandwiched Nujol mulls (500–100 cm^{-1}). Mass spectra were obtained with a Hewlett Packard HP598A spectrometer. Electronic spectra were obtained with a Shimadzu UV-3101PC spectrophotometer equipped with a reflectance accessory. X-band EPR spectra of the complexes were obtained in 3 mm Pyrex tubes with a Bruker EMX spectrometer using

a conventional Dewar insert at liquid nitrogen temperature and Cr^{II} as the reference. Room temperature magnetic moments were determined on a DSM-8 magnetic susceptibility balance, and the instrument was calibrated using nickel metal. Variable-temperature (5–293 K) magnetic susceptibility measurements on a polycrystalline sample of **5a** were carried out with a Quantum Design SQUID susceptometer using an applied magnetic field of 2000 G over the whole temperature range. All data were corrected for diamagnetism of the ligands as estimated from Pascal's constants. The conductivity measurements were carried out with a CRISON digital conductivity bridge model MicroCM 2202 using freshly prepared 10^{-3} M solutions of the complexes in DMF. Thermogravimetric analysis from 20 to 950 °C was performed in a Shimadzu TGA-DGT 50H thermobalance using a constant 100 mL/min air flow. Evolved gases were identified from between 21 and 24 IR spectra of the gaseous products that were recorded at appropriate times during the analysis using a coupled Nicolet Magma 550 FTIR spectrophotometer; in each spectrum, the characteristic bands of the various gases were unequivocally identified by comparison with spectra in the Sigma–Aldrich FTIR library. Cyclic voltammograms were obtained on a 273 EG&G Princeton Applied Research electrochemical analyzer. The measurements were carried out at 50 mV·s^{-1} under oxygen-free conditions using a three-electrode cell with a glassy carbon electrode. Tetra(*n*-butyl)ammonium perchlorate (TBAP) was used as the supporting electrolyte.

All chemicals and solvents were of analytical grade and were used as received. The TBAP used as the supporting electrolyte in electrochemical measurements was purchased from Fluka and recrystallized from hot methanol.

Caution! Perchlorates are potentially explosive and care should be taken in handling these compounds.

Preparation of HAm4DH: The ligand, HAm4DH, 2-pyridineformamide thiosemicarbazone was prepared according to a literature procedure.[2]

Synthesis of [Cu(HAm4DH)Cl$_2$] (1): An ethanolic solution (20 mL) of HAm4DH (0.25 g, 1.28 mmol) was added to a stirred solution of $CuCl_2 \cdot 2H_2O$ (0.22 g, 1.28 mmol) in ethanol (20 mL). The mixture was stirred for 7 days; the resulting suspension was filtered off and the bluish-green solid was washed with ethanol and dried with calcium chloride. Yield: 0.38 g (90%). $C_7H_9Cl_2CuN_5S$ (329.70): calcd. C 25.5, H 2.8, N 21.2, S 9.7; found C 25.6, H 2.8, N 21.0, S 9.5. Selected IR data: $\tilde{\nu}_{max}$ = 3437–3165 (NH), 1639–1578 (C=N + C=C), 1020 (NN), 793 (C=S), 463 (Cu–N), 349 (Cu–S), 319, 264 (Cu–Cl) cm^{-1}. FAB$^+$ MS [*m*/*z*, assignment]: 258 [Cu(HAm4DH)]. UV/Vis (λ_{max}, nm): 26738, 24154, 15244, 14245. EPR (X-band, solid sample): $g_{\parallel}$ = 2.19, $g_{\perp}$ = 2.04, g_{av} = 2.05, G = 4.75. μ_{eff} = 2.05 MB. Conductance (Λ_m/S·cm^2·mol^{-1}) in DMF: 28.

Synthesis of [Cu(HAm4DH)Br$_2$]·0.5 EtOH·0.5 H$_2$O (2): A solution of HAm4DH (0.20 g, 1.02 mmol) in ethanol (20 mL) was added to a solution of $CuBr_2$ (0.46 g, 2.05 mmol) in ethanol (20 mL). The mixture was stirred for one week and the resulting dark brown solid was filtered off, washed with ethanol, and dried under vacuum. Yield: 0.92 g (99%). $C_8H_{13}Br_2CuN_5OS$ (545.64): calcd. C 21.3, H 2.9, N 15.5, S 7.1; found C 22.2, H 2.3, N 15.0, S 6.5. Selected IR data: $\tilde{\nu}_{max}$ = 3408, 3324 (NH), 1562, 1515 (C=N, C=C), 1015 (NN), 789 (C=S), 464 (Cu–N2), 324 (Cu–S), 254 (Cu–Br) cm^{-1}. FAB$^+$ MS [*m*/*z*, assignment]: 338, [Cu(Am4DH)Br]; 257, [Cu(Am4DH)]. UV/Vis (λ_{max}, nm): 26693, 24232, 15253, 14271 cm^{-1}. EPR (X-band, solid sample): g_{iso} = 2.04. μ_{eff} = 2.16 MB. Conductance (Λ_m/S·cm^2·mol^{-1}) in DMF: 34.6.

Synthesis of [Cu(HAm4DH)$_2$](NO$_3$)$_2$·EtOH (3): A solution of $Cu(NO_3)_2 \cdot 3H_2O$ (0.25 g, 1.02 mmol) and HAm4DH (0.40 g, 2.05 mmol) in ethanol (20 mL) was stirred for one week. A dark green precipitate formed and this was filtered off, washed with ethanol, and dried under vacuum. Yield: 0.25 g (40%). $C_{16}H_{24}CuN_{12}O_7S_2$ (624.11): calcd. C 30.8, H 3.9, N 26.9, S 10.3; found C 31.5, H 3.5, N 26.2, S 11.8. Selected IR data : $\tilde{\nu}_{max}$ = 3422–3171 (NH), 1599–1519 (C=N, C=C), 1384 (NO_3), 1016 (NN), 840 (C=S), 467 (Cu–N2), 338 (Cu–S) cm^{-1}. FAB$^+$ MS [*m*/*z*, assignment]: 453, [Cu(HAm4DH)$_2$]; 322, [Cu(H$_3$Am4DH)(NO$_3$)]; 259, [Cu(H$_2$Am4DH)]. UV/Vis (λ_{max}, nm): 26378, 22676, 21459, 16326, 15588. EPR (X-band, solid sample): g_{iso} = 2.08. μ_{eff} = 2.16 MB. Conductance (Λ_m/S·cm^2·mol^{-1}) in DMF: 125.6.

Synthesis of [Cu(HAm4DH)$_2$](ClO$_4$)$_2$ (4): A solution of HAm4DH (0.25 g, 1.28 mmol) in ethanol (20 mL) was added to a solution of $Cu(ClO_4)_2 \cdot 6H_2O$ (0.47 g, 1.28 mmol) in ethanol (20 mL). The mixture was stirred for 7 days and the resulting black solid was filtered off, washed with ethanol and dried with calcium chloride. Yield: 0.64 g (76%). $C_{14}H_{18}Cl_2CuN_{10}O_8S_2$ (652.93): calcd. C 23.5, H 2.3, N 19.6, S 9.0; found C 23.9, H 2.4, N 19.3, S 9.0. Selected IR data: $\tilde{\nu}_{max}$ = 3421–3189 (NH), 1619–1518 (C=N, C=C), 1118, 936, 632 [ν_3, ν_1, ν_4 (ClO_4)], 1019 (NN), 847 (C=S), 488 (Cu–N2), 363 (Cu–S) cm^{-1}. FAB$^+$ MS [*m*/*z*, assignment]: 258, [Cu(HAm4DH)]. UV/Vis (λ_{max}, nm): 26364, 22655, 15593, 14290. EPR (X-band, solid sample): $g_{\parallel}$ = 2.19, $g_{\perp}$ = 2.04, g_{av} = 2.08, G = 4.75. μ_{eff} = 1.97 MB. Conductance (Λ_m/S·cm^2·mol^{-1}) in DMF: 152.4.

Synthesis of [Cu(Am4DH)Cl]·0.5 EtOH (5): A solution of HAm4DH (0.20 g, 1.02 mmol) in ethanol was added to a stirred solution of $CuCl_2 \cdot 2H_2O$ (0.18 g, 1.02 mmol) in ethanol (20 mL). After a few drops of triethylamine (0.14 mL, 1.02 mmol) were added, the mixture was stirred for 7 days, just to complete precipitation of a dark green solid which was filtered off, washed with ethanol, and dried. Yield: 0.30 g (92%). $C_8H_{11}ClCuN_5O_{0.5}S$ (316.27): calcd. C 30.4, H 3.5, N 22.1, S 10.1; found C 30.2, H 3.5, N 21.7, S, 9.4. Selected IR data: $\tilde{\nu}_{max}$ = 3473–3158 (NH), 1625–1515 (C=N, C=C), 1020 (NN), 783 (C=S), 467 (Cu–N2), 350 (Cu–S), 313 (Cu–Cl) cm^{-1}. FAB$^+$ MS [*m*/*z*, assignment]: 294, [Cu(H$_2$Am4DH)Cl]; 259, [Cu(H$_2$Am4DH)]. UV/Vis (λ_{max}, nm): 26385, 22989, 16247, 15662 cm^{-1}. EPR (X-band, solid sample): g_{iso} = 2.08. μ_{eff} = 2.04 MB. Conductance (Λ_m/S·cm^2·mol^{-1}) in DMF: 47.8. Recrystallization from MeOH/CCl_4 or EtOH/H_2O gave green prismatic crystals of [Cu(HAm4DH)Cl$_2$]$_2$ (**5a**) and green needles of $^1_\infty$[Cu(Am4DH)Cl] (**5b**), respectively, that were suitable for X-ray diffraction.

Synthesis of [Cu(Am4DH)Br]·0.5 EtOH (6): A solution of HAm4DH (0.20 g, 1.02 mmol) in ethanol (20 mL) was added to a solution of $CuBr_2$ (0.23 g, 1.02 mmol) in ethanol (20 mL). Triethylamine (0.14 mL, 1.02 mmol) was added and the mixture was stirred for one week. The resulting dark green solid was filtered off, washed with ethanol, and dried under vacuum. Yield: 0.31 g (84%). $C_8H_{11}BrCuN_5O_{0.5}S$ (360.72): calcd. C 26.6, H 3.1, N 19.4, S 8.9; found C 26.7, H 3.0, N 19.2, S 6.2. Selected IR data: $\tilde{\nu}_{max}$ = 3521–3159 (NH), 1613–1514 (C=N, C=C), 1017 (NN), 844 (C=S), 468 (Cu–N2), 329 (Cu–S), 255 (Cu–Br) cm^{-1}. FAB$^+$ MS [*m*/*z*, assignment]: 338, [Cu(Am4DH)Br]; 257, [Cu(Am4DH)]. UV/Vis (λ_{max}, nm): 26350, 23068, 16247, 15698 cm^{-1}. EPR (X-band, solid sample): g_{iso} = 2.07. μ_{eff} = 1.98 MB. Conductance (Λ_m/S·cm^2·mol^{-1}) in DMF: 62.6. X-ray quality crystals of $^1_\infty$[Cu(Am4DH)Br] (**6a**) were obtained as blue prisms by recrystallization from MeOH/acetonitrile.

Synthesis of [Cu(Am4DH)(OAc)] (7): A solution of HAm4DH (0.20 g, 1.02 mmol) in ethanol (20 mL) was added to a solution of $Cu(CH_3OO)_2 \cdot H_2O$ (0.20 g, 1.02 mmol) in ethanol (20 mL) and triethylamine was added (0.14 mL, 1.02 mmol). The mixture was

stirred for 7 days and the resulting green solid was filtered off, washed with ethanol, and dried under vacuum. Yield: 0.26 g (80%). $C_9H_{11}CuN_5O_2S$ (316.83): calcd. C 34.1, H 3.5, N 22.1, S 10.1; found C 34.4, H 3.5, N 21.8, S 10.0. Selected IR data: $\tilde{\nu}_{max}$ = 3427–3183 (NH), 1596, 1515 (C=N, C=C, CH_3COO), 1407 (CH_3COO), 1018 (NN), 846 (C=S), 442 (Cu–N2), 409 (Cu–O), 351 (Cu–S) cm^{-1}. FAB^+ MS [*m*/*z*, assignment]: 257, [Cu(Am4DH)]. UV/Vis (λ_{max}, nm): 26399, 23364, 16155, 15662, 14358 cm^{-1}. EPR (X-band, solid sample): $g_{\parallel}$ = 2.20, $g_{\perp}$ = 2.04, g_{av} = 2.06, G = 5. μ_{eff} = 2.10 MB. Conductance (Λ_m/S·cm²·mol⁻¹) in DMF: 33.7.

Synthesis of [Cu(Am4DH)(NO$_3$)]·0.5 EtOH (8): A solution of HAm4DH (0.20 g, 1.02 mmol) in ethanol was added to a stirred solution of $Cu(NO_3)_2{\cdot}3H_2O$ (0.25 g, 1.02 mmol) in ethanol (20 mL). After adding a few drops of triethylamine (0.14 mL, 1.02 mmol), the mixture was stirred for 7 days and, a dark brown solid was isolated that was filtered off, washed with ethanol, and dried with calcium chloride. Yield: 0.27 g (77%). $C_8H_{13}CuN_6O_{3.5}S$ (342.82): calcd. C 28.0, H 3.2, N 24.5, S 9.4; found C 27.5, H 2.9, N 24.8, S 10.2. Selected IR data: $\tilde{\nu}_{max}$ = 3424–3172 (NH), 1598–1523 (C=N, C=C), 1384, 1101 (NO_3), 1016 (NN), 841 (C=S), 465 (Cu–N2), 333 (Cu–S) cm^{-1}. FAB^+ MS [*m*/*z*, assignment]: 320, [Cu(HAm4DH)(NO_3)]; 257, [Cu(Am4DH)]. UV/Vis (λ_{max}, nm): 26406, 23474, 21186, 16353, 15785 cm^{-1}. EPR (X-band, solid sample): $g_{\parallel}$ = 2.20, $g_{\perp}$ = 2.04, g_{av} = 2.05, G = 5. μ_{eff} = 2.15 MB. Conductance (Λ_m/S·cm²·mol⁻¹) in DMF: 40.2.

Synthesis of [Cu(Am4DH)(H$_2$O)](ClO$_4$) (9): A solution of HAm4DH (0.20 g, 1.02 mmol) in ethanol was added to a stirred solution of $Cu(ClO_4)_2{\cdot}6H_2O$ (0.38 g, 1.02 mmol) in ethanol (20 mL). After adding a few drops of triethylamine (0.14 mL, 1.02 mmol), the mixture was stirred for 7 days and the brown solid formed was filtered off, washed with ethanol, and dried. Yield: 0.16 (43%). $C_7H_{10}ClCuN_5O_5S$ (375.25): calcd. C 22.4, H 2.7, N 18.7, S 8.5; found C 22.2, H 2.4, N 16.2, S 7.8. Selected IR data: $\tilde{\nu}_{max}$ = 3429–3175 (NH), 1608–1518 (C=N, C=C), 1109, 926, 627 [ν_3, ν_1, ν_4 (ClO_4)], 1016 (NN), 791 (C=S), 466 (Cu–N), 350 (Cu–S) cm^{-1}. FAB^+ MS [*m*/*z*, assignment]: 255, [Cu(Am4DH-2 H)]. UV/Vis (λ_{max}, nm): 26716, 23252, 15964, 15431. μ_{eff} = 2.19 MB. Conductance (Λ_m/S·cm²·mol⁻¹) in DMF: 90.3. Dark green prismatic crystals of [Cu(HAm4DH)(H_2O)(ClO_4)$_2$]·MeOH·H_2O (**9a**) suitable for X-ray diffractometry were obtained after a few days by slow evaporation of a mixture of MeOH/CCl_4 at room temperature.

Synthesis of [Cu(Am4DH)$_2$]·4 H$_2$O (10): $Cu(CH_3OO)_2{\cdot}H_2O$ (0.20 g, 1.02 mmol) and HAm4DH (0.4 g, 2.05 mmol) were dissolved in ethanol (20 mL); some triethylamine was added (0.28 mL, 2.05 mmol) and the mixture was stirred for a week. The dark green precipitate was filtered off, washed with ethanol, and dried under vacuum. Yield: 0.35 (42%). $C_{14}H_{24}CuN_{10}O_4S_2$ (524.08): calcd. C 32.1, H 4.6, N 26.7, S 11.2; found C 32.1, H 3.3, N 25.2, S 13.7. Selected IR data: $\tilde{\nu}_{max}$ = 3423–3174 (NH), 1598–1520 (C=N, C=C), 1016 (NN), 845 (C=S), 470 (Cu–N2), 337 (Cu–S) cm^{-1}. FAB^+ MS [*m*/*z*, assignment]: 452, [Cu(HAm4DH)(Am4DH)]; 257, [Cu(Am4DH)]. UV/Vis (λ_{max}, nm): 26724, 22624, 15649, 14409 cm^{-1}. EPR (X-band, solid sample): g_{iso} = 2.08. μ_{eff} = 2.13 MB. Conductance (Λ_m/S·cm²·mol⁻¹) in DMF: 32.7.

X-ray Crystallography: Crystals were mounted on glass fibers and these samples were used for data collection. Data for **5b** and **6a** were collected with a Nonius CAD4 automatic diffractometer and for **5a** and **9a** with a Bruker SMART CCD 1000 diffractometer. Cell constants and an orientation matrix were obtained from data collection of $2.03 < \theta < 26.48°$ for **5a**, $15.69 < \theta < 45.59°$ for **5b**,

Table 6. Crystal data and structure refinement for **5a**, **5b**, **6a**, and **9a**.

Compound	**5a**	**5b**	**6a**	**9a**
Empirical formula	$C_{14}H_{18}Cl_4Cu_2N_{10}S_2$	$C_7H_8ClCuN_5S$	$C_7H_8BrCuN_5S$	$C_8H_{17}Cl_2CuN_5O_{11}S$
Formula weight	659.38	293.23	337.69	525.77
Temperature [K]	293(2)	293(2)	293(2)	150(2)
Wavelength [Å]	0.71073	1.54184	1.54184	0.71073
Crystal system	monoclinic	orthorhombic	orthorhombic	triclinic
Space group	$P2_1/c$ (no. 14)	*Pbcn* (no. 60)	*Pbcn* (no. 60)	$P\bar{1}$ (no. 2)
a [Å]	10.660(2)	20.2564(8)	19.8492(13)	11.243(3)
b [Å]	10.865(2)	7.5598(3)	7.7764(6)	12.662(3)
c [Å]	10.812(2)	15.0873(7)	15.2852(13)	13.539(3)
α [°]	90	90	90	80.230(3)
β [°]	109.377(3)	90	90	78.177(3)
γ [°]	90	90	90	86.411(4)
Volume [Å^{-3}]	1181.3(4)	2310.4(2)	2359.4(3)	1858.4(8)
Z	2	8	8	4
ρ_{calcd} [Mg·m^{-3}]	1.854	1.686	1.901	1.879
Abs. coefficient [mm^{-1}]	2.456	6.295	8.050	1.641
F (000)	660	1176	1320	1068
Crystal size	0.51 × 0.47 × 0.27	0.48 × 0.12 × 0.02	0.48 × 0.24 × 0.08	0.58 × 0.49 × 0.17
θ range [°]	2.03–26.48	4.37–72.89	4.46–72.89	1.56–26.43
Limiting indices *h*, *k*, *l*	–12/13, 0/13, –13/0	0/24, –9/0, –18/0	–24/0, 0/9, 0/18	–13/14, –15/15, 0/16
Reflections collected	9947	2975	3025	21117
Unique reflections/R_{int}	2427/0.0203	2314/0.0553	2361/0.0532	7577/0.0188
Absorp. correct.	SADABS	*Ψ*-scans	*Ψ*-scans	SADABS
Max./min. transmission	0.5569/0.3673	0.8844/0.1521	0.5653/0.1131	0.7677/0.4494
Data/parameters	2427/145	2314/136	2361/136	7577/505
Gof (for F^2)	1.078	0.988	1.058	1.045
Final *R* indices [$I > 2\sigma(I)$]	R_1 = 0.0268	R_1 = 0.0699	R_1 = 0.0481	R_1 = 0.0425
	wR_2 = 0.0714	wR_2 = 0.1872	wR_2 = 0.1400	wR_2 = 0.1070
R indices (all data)	R_1 = 0.0379	R_1 = 0.1412	R_1 = 0.1561	R_1 = 0.0635
	wR_2 = 0.0793	wR_2 = 0.2064	wR_2 = 0.1427	wR_2 = 0.1239
Larg. diff. peak/hole [e·Å^{-3}]	0.560/–0.335	0.655/–0.637	0.904/–1.314	2.182/–1.292

$1.56 < \theta < 26.43°$ for **6a** and $4.37 < \theta < 72.98°$ for **9a**. The data for **5b** and **6a** were processed with SAINT[45] and corrected for absorption using SADABS.[46] The structures were solved by direct methods,[47] which revealed the position of all non-hydrogen atoms. These atoms were refined on F^2 by a full-matrix least-squares procedure using anisotropic displacement parameters.[48] The hydrogen atoms were located from difference syntheses or in their calculated positions (C–H, 0.93–0.97 Å), and were refined using a riding model. Atom scattering factors were taken from the International Tables for Crystallography.[49] Crystal and refinement data are listed in Table 6.

Cleavage of pUV18 by Thiosemicarbazone/Copper: The interaction of the copper(II) complexes with DNA was studied using the plasmid pUC18 in the presence of H_2O_2, with the resulting fragments analyzed by electrophoresis in agarose. Plasmid pUC18 has a size of 2686 base pairs at a concentration of 0.25 mg·mL^{-1} in TE buffer (pH = 8, Tris 10 mM, EDTA 1 mM). The assay carried out involved digesting plasmid pUC18 with the copper complexes in the presence of a reducing agent. The copper(II) complexes are insoluble in the buffer solutions commonly used in DNA degradation processes. For this reason DMF was employed as a solvent and the method reported by Reddy[50] was used for studies in this solvent. A typical assay was carried out as follows: 7 μL of 0.1 M cacodylate buffer (pH = 6.0), 1 μL of DNA pUC18 (0.25 μg·μL^{-1}), 6 μL of a solution of the copper(II) complex (or copper) (40 or 80 μM) in 0.1 M cacodylate buffer (pH = 6.0), 3 μL of H_2O_2 (0.4 or 0.8 mM) in 0.1 M cacodylate buffer, and 3 μL ascorbate (0.4 or 0.8 mM). The samples were incubated at 37 °C for 60 min. After this time 3 μL of charge buffer (0.25% bromophenol, 0.25% xylene cyanol, and 30% glycerol) was added and the electrophoresis was carried out immediately at 80 V in 0.8% agarose gel [containing 2 μL/100 mL of a solution of ethidium bromide (10 mg·mL^{-1})] using 0.5×TBE as a buffer (0.045 M Tris, 0.045 M boric acid, and 1 mM EDTA) for 2–2.5 h. The gel was photographed using a Gel printer Plus TDI system. Assays involving the various inhibitors were carried out in the same way as above but the agents under investigation were added as follows: *tert*-butyl alcohol (1 M) and DMSO (1 M) for their ability to scavenge OH· radicals, sodium azide (100 mM), and 2,2,6,6-tetramethyl-4-piperidone (100 mM), which are characterized by their ability to scavenge singlet oxygen; distamycin (8 mM), which intercalates between the nucleobases of the minor groove of the double helix of DNA and superoxide dismutase (15 units) for its ability to quench the superoxide radical. It is known that copper(II) shows nuclease activity in its own right and therefore comparative electrophoresis was carried out for a range of incubation times in order to determine whether the complex showed higher, lower or equivalent activity to the copper(II) salts.

CCDC-277157 (for $[Cu(HAm4DH)Cl_2]_2$), CCDC-277158 (for $^1_\infty[Cu(Am4DH)Cl]$), CCDC-277159 for ($^1_\infty[Cu(Am4DH)Br]$), and CCDC-277160 for ($[Cu(HAm4DH)(H_2O)(ClO_4)_2]$·MeOH·$H_2O$) contain the supplementary crystallographic data for this paper. These data can be obtained free of charge from The Cambridge Crystallographic Data Centre via www.ccdc.cam.ac.uk/data_request/cif.

Acknowledgments

Financial support from ERDF (EU)-DGI-MCYT (Spain) (Projects BQU2002-04523-C02 and CTQ2004-03735) and the Xunta de Galicia (Project PGIDIT03PXIC20302PN) is gratefully acknowledged.

[1] a) D. X. West, A. E. Liberta, S. B. Padhye, R. C. Chikate, P. B. Sonawane, A. S. Kumbhar, R. G. Yerande, *Coord. Chem. Rev.* **1993**, *123*, 49–71; b) D. X. West, S. B. Padhye, P. B. Sonawane, *Struct. Bonding* **1991**, *76*, 1–50.
[2] P. J. Van Koningsbruggen, J. G. Haasnoot, R. A. G. de Graalf, J. Reedijk, *Inorg. Chim. Acta* **1995**, *234*, 87–94.
[3] J. García-Tojal, J. García-Jaca, R. Cortés, T. Rojo, M. K. Urtiaga, M. I. Arriortua, *Inorg. Chim. Acta* **1996**, *249*, 25–32.
[4] A. G. Bingham, H. Bögge, A. Müller, E. W. Ainscough, A. M. Brodie, *J. Chem. Soc., Dalton Trans.* **1987**, 493–499.
[5] E. W. Ainscough, A. M. Brodie, J. D. Ranford, J. M. Waters, *J. Chem. Soc., Dalton Trans.* **1991**, 1737–1742.
[6] E. W. Ainscough, A. M. Brodie, J. D. Ranford, J. M. Waters, K. S. Murray, *Inorg. Chim. Acta* **1992**, *197*, 107–115.
[7] J. García Tojal, M. K. Yrtiaga, R. Cortés, L. Lezama, M. I. Arriortua, T. Rojo, *J. Chem. Soc., Dalton Trans.* **1994**, 2233–2238.
[8] C. F. Bell, C. R. Theocharis, *Acta Crystallogr., Sect. C* **1987**, *43*, 26–29.
[9] A. Castiñeiras, I. García-Santos, E. Bermejo, D. X. West, *Z. Naturforsch., Teil B* **2000**, *B55*, 511–518.
[10] A. Castiñeiras, I. García-Santos, E. Bermejo, D. X. West, *Polyhedron* **2000**, *19*, 1873–1880.
[11] I. García-Santos, A. Hagenbach, U. Abram, *Dalton Trans.* **2004**, 677–682.
[12] I. García-Santos, U. Abram, R. Alberto, E. Vazquez-López, *Inorg. Chem.* **2004**, *43*, 1834–1836.
[13] D. X. West, J. K. Swearingen, J. Valdés-Martínez, S. Hernández-Ortega, A. K. El-Sawaf, F. van Meurs, A. Castiñeiras, I. García-Santos, E. Bermejo, *Polyhedron* **1999**, *18*, 2919–2929.
[14] I. García-Santos, E. Bermejo, A. K. El-Sawaf, A. Castiñeiras, D. X. West, *Polyhedron* **2002**, *21*, 729–737.
[15] E. Bermejo, A. Castiñeiras, L. M. Fostiak, I. García-Santos, A. L. Llamas-Saiz, J. K. Swearingen, D. X. West, *Z. Naturforsch. B* **2001**, *56*, 1297–1305.
[16] L. M. Fostiak, I. García-Santos, J. K. Swearingen, E. Bermejo, A. Castiñeiras, D. X. West, *Polyhedron* **2003**, *22*, 83–92.
[17] E. Bermejo, A. Castiñeiras, I. García-Santos, D. X. West, *Polyhedron* **2003**, *22*, 1147–1154.
[18] I. García-Santos, U. Abram, *Z. Anorg. Allg. Chem.* **2004**, *630*, 697–700.
[19] A. Castiñeiras, I. García-Santos, E. Bermejo, K. A. Ketcham, D. X. West, A. K. El-Sawaf, *Z. Anorg. Allg. Chem.* **2002**, *628*, 492–504.
[20] E. Bermejo, A. Castiñeiras, I. García-Santos, D. X. West, *Z. Allg. Anorg. Chem.* **2005**, *631*, 2011–2019.
[21] K. A. Ketcham, I. García-Santos, J. K. Swearingen, E. Bermejo, A. K. El-Sawaf, A. Castiñeiras, D. X. West, *Polyhedron* **2002**, *21*, 859–865.
[22] K. A. Ketcham, J. K. Swearingen, A. Castiñeiras, I. García-Santos, E. Bermejo, D. X. West, *Polyhedron* **2001**, *20*, 3265–3273.
[23] K. A. Ketcham, I. García-Santos, E. Bermejo, J. K. Swearingen, A. Castiñeiras, D. X. West, *Z. Anorg. Allg. Chem.* **2002**, *628*, 409–415.
[24] W. J. Geary, *Coord. Chem. Rev.* **1971**, *7*, 81–122.
[25] M. B. Ferrari, G. G. Fava, P. Tarasconi, C. Pelizzi, *J. Chem. Soc., Dalton Trans.* **1989**, 361–366.
[26] P. G. Beckingsale, A. T. Morcom, C. E. F. Rickard, T. N. Waters, *J. Chem. Soc., Dalton Trans.* **1977**, 2135–2138.
[27] P. De Meester, A. C. Skapski, *J. Chem. Soc., Dalton Trans.* **1972**, 2400–2404.
[28] a) E. D. Estes, W. E. Estes, W. E. Hatfield, D. J. Hodgson, *Inorg. Chem.* **1975**, *14*, 106–109; b) D. D. Swank, G. F. Needham, R. D. Willet, *Inorg. Chem.* **1979**, *18*, 761–765.
[29] D. X. West, J. K. Swearingen, T. J. Romack, I. S. Billeh, J. P. Jasinski, Y. Li, R. J. Staples, *J. Mol. Struct.* **2001**, *570*, 129–136.

[30] M. A. Ali, K. K. Dey, M. Nazimuddin, F. E. Smith, R. J. Butcher, J. P. Jasinski, J. M. Jasinski, *Polyhedron* **1996**, *15*, 3331–3339.
[31] W. E. Marsh, W. E. Hatfield, D. J. Hodgson, *Inorg. Chem.* **1982**, *21*, 2679–2684.
[32] D. J. Hodgson, P. K. Hale, W. E. Hatfield, *Inorg. Chem.* **1971**, *10*, 1061–1067.
[33] Y.-M. Lee, H.-W. Lee, Y.-I. Kim, *Polyhedron* **2005**, *24*, 377–382.
[34] A. W. Addison, T. N. Rao, J. Reedijk, J. V. Rijn, G. C. Verschoor, *J. Chem. Soc., Dalton Trans.* **1984**, 1349–1356.
[35] A. W. Addison, T. N. Rao, E. Sinn, *Inorg. Chem.* **1984**, *23*, 1957–1967.
[36] G. A. Lawrance, B. W. Skelton, A. H. White, *Aust. J. Chem.* **1986**, *39*, 1101–1108.
[37] S. C. Bhatia, A. K. Chatrath, P. C. Jain, *J. Indian Chem. Soc.* **1997**, *74*, 769–771.
[38] A. B. P. Lever, *Inorganic Electronic Spectroscopy*, 2nd ed., Elsevier, Amsterdam, **1986**.
[39] B. Bleaney, K. D. Bowers, *Proc. R. Soc. London, Ser. A* **1952**, *214*, 451–465.
[40] E. A. Boudreaux, L. N. Mulay, *Theory and Applications of Molecular Magnetism*, John Wiley & Sons, New York, **1976**.
[41] a) W. E. Hatfield, *Comments Inorg. Chem.* **1981**, *1*, 105–121; b) W. E. Marsh, K. C. Patel, W. I. Hatfield, D. J. Hodgson, *Inorg. Chem.* **1983**, *22*, 511–515; c) W. A. Alves, R. H. de Almeida Santos, A. Paduan-Filho, C. C. Becerra, A. C. Borin, A. M. Da Costa Ferreira, *Inorg. Chim. Acta* **2004**, *357*, 2269–2278.
[42] R. Rodríguez, A. Llobet, M. Corbello, A. E. Martell, J. Reibenspies, *Inorg. Chem.* **1999**, *38*, 2328–2334.
[43] P. Kapoor, A. Pathak, R. Kapoor, P. Venugopalan, M. Corbella, R. Rodríguez, J. Roblew, A. Llobet, *Inorg. Chem.* **2002**, *41*, 6153–6160.
[44] A. S. Kumbhar, S. S. Padhye, D. X. West, A. E. Liberta, *Transition Met. Chem.* **1991**, *16*, 276–279.
[45] Bruker, SMART and SAINT. *Area Detector Control Integration Software*, Bruker Analytical X-ray Instruments, Inc., Madison, WI, **1999**.
[46] G. M. Sheldrick, *SADABS, Program for Empirical Absorption Correction of Area Detector Data*, University of Göttingen, Germany, **1997**.
[47] G. M. Sheldrick, *Acta Crystallogr., Sect. A* **1990**, *46*, 467–473.
[48] G. M. Sheldrick, *SHELX-97, Program for the Refinement of Crystal Structures*, University of Göttingen, Germany, **1997**.
[49] A. J. C. Wilson (Ed.), *International Tables for Crystallography*, Kluwer Academic Publishers, Dordrecht, **1995**, vol. C.
[50] K. H. Reddy, P. S. Reddy, *Transition Met. Chem.* **2000**, *25*, 505–510.

Received: September 8, 2005
Published Online: January 19, 2006

